

On the drape and level flying aeromagnetic survey modes with terrain effects, and data reduction between arbitrary surfaces

Yunus Levent EKİNCİ^{1,2,*} 

¹Department of Archaeology, Faculty of Science and Arts, Bitlis Eren University, Bitlis, Turkey

²Career Application and Research Center, Bitlis Eren University, Bitlis, Turkey

Received: 21.07.2020 • Accepted/Published Online: 27.12.2020 • Final Version: 17.05.2021

Abstract: In addition to the physical parameters such as magnetization intensity distribution, the volume and the shape of the magnetized material, directions of the magnetization and the ambient field, the distance between the observation surface and the causative sources significantly affects the shape and the amplitudes of the magnetic anomalies. Aeromagnetic surveys are performed using either a draped surface or a constant elevation plane above sea level. These surveys can easily reconnoiter large territories in a short time. However, the magnetic anomalies may be attenuated resulting in some losses in the data resolution based on the flight height of the survey. In this paper, these effects were investigated in a detailed manner through some synthetic anomalies generated from 2D and 3D hypothetical subsurface models. Besides, magnetic terrain effects were also examined in the synthetic simulations which were produced for different scenarios. Real aeromagnetic anomalies obtained using a drape flying survey mode over the rugged high topographic relief of the Mount Nemrut stratovolcano (Bitlis, eastern Turkey) and its close vicinity were also investigated. Numerical simulations show that although both data acquisition modes have some weak sides, the level flying mode is more advantageous than the drape flying mode in general. Better anomaly interpretation can be achieved by reducing the draped data set into the one observed over a horizontal plane or vice versa and comparing these two data sets. Lastly, a simple computational process which can be performed in the Fourier wavenumber domain is proposed for data reduction procedure.

Key words: Aeromagnetic survey, drape flying, level flying, terrain effect, uneven surface, data reduction

1. Introduction

After the invention of the first electronically designed magnetometers in the World War II, aeromagnetic/airborne magnetic surveys started to be used for the detection of submarines (Blakely, 1996; Reeves, 2005). The first detailed aeromagnetic survey was performed in 1944 by the US Geological Survey for a petroleum reserve which is located in Alaska (Hildenbrand and Raines, 1987). Since then aeromagnetic surveys have been frequently performed at many scales for a great variety of purposes. In aeromagnetic surveys, a helicopter or an airplane carrying a magnetometer flies back-and-forth and uses a grid-like flight route. Thus, usually, equally spaced parallel flight lines are preferred over the studied regions (Robinson and Çoruh, 1988). Reconnoitering large territories in a very short time and also minimizing the possible undesired effects caused by cultural features, temporal changes and surface geology are the main advantages of the aeromagnetic surveying (Hinze et al., 2013). Observation heights, profile distances, and the data sampling intervals significantly affect the resolution of the obtained anomaly.

* Correspondence: ylekinici@beu.edu.tr

As the distance between the observation height and the anomaly sources is increased, some possible losses in the data resolution are expected (Zhou, 2018). Hence, compared with the ground-based magnetic surveys, generally higher sensitivity magnetometers are used in the aeromagnetic surveys (Lowrie, 2007). Additionally, aeromagnetic surveying procedures are more complicated than ground-based surveying, and therefore much more corrections are carried out.

In aeromagnetic surveys, two types of flying modes are used. Drape flying or draped surveying mode uses a constant terrain clearance in which the distance is the same from the ground surface while level flying mode uses a constant elevation above sea level. Over the gentle sloping territories both of the flying modes can be preferred. However, in the mountainous regions with highly rugged topographies a constant elevation above sea level is generally preferred, and level flying mode is used for the safety of the flying. These two flying modes have both some advantages and disadvantages over each other (Pilkington and Roest, 1992). However, there are some

contradictory statements on this subject. Contrarily to the general belief, Grauch and Campell (1984) reported that drape flying surveys can strengthen magnetic terrain anomaly problems. However, this explanation is not completely true when we consider the amplitude differences between the strongly and weakly magnetized terrains. But it must be noted that abrupt topographic changes may cause too severe spurious phases in the aeromagnetic anomalies. Walls and Hall (1998) stated that these effects are expected to be small and negligible over strongly magnetized topographies. In opposition to this statement, Pilkington and Thurston (2001) reported that these undesired effects are particularly serious in the presence of a strongly magnetized near-surface material. On the other hand, Ridsdill-Smith and Dentith (2000) stated that drape flying surveys are commonly performed to reduce the magnetic effects of variable terrain clearance. Nowadays, except for rare exceptions, aeromagnetic surveys are performed using draped/uneven surfaces with the same distance with respect to the ground surface (Pilkington and Boulanger, 2017). However, this case is more challenging and complicated, and also poses a significant methodological problem. It is well known that data processing grid operations which are performed in the wavenumber domain are suitable for level data sets. This means that if fast Fourier transform-based data processing techniques such as analytical continuations, phase transformations, filtering, linear transformations, spectral analyses, computation of directional derivatives and vertical integrals, etc. are performed for draped data without performing proper modifications deceptive results are generally obtained. To overcome this problem, draped data must be reduced to a horizontal plane/level. Additionally, this datum plane must coincide over the highest topography and the observation height (Tivey at al., 1993; Szitkar and Dymont, 2015; Ekinici et al., 2020).

In this study, the effects of the drape and level flying surveying modes on the aeromagnetic anomalies were examined by using some 2D and 3D hypothetical subsurface models. Magnetic terrain effects were also investigated in the numerical simulations. Moreover, real aeromagnetic anomalies observed over the Mount Nemrut stratovolcano (Bitlis, Eastern Turkey) and its close vicinity were analyzed. The validness and the reliability of an alternative easy wavenumber domain computational procedure for the data reduction process was also presented. All the computations used here were performed via a MATLAB-based potential field data processing package (Ekinici, 2010; Ekinici and Yiğitbaş, 2012, 2015).

2. Forward problem

The total field magnetic anomaly of a vertically positioned prismatic block with a bottom at infinity can be

approximated by using the expression given below (Leite and Leao, 1985)

$$\Delta T = 2J_j \left[A_{oj} \arctan\left(\frac{C_{ij}}{z_j}\right) - \arctan\left(\frac{D_{ij}}{z_j}\right) \right] + \frac{1}{2} B_{oj} \ln\left(\frac{E_{ij}}{F_{ij}}\right) + T_0, \quad (1)$$

where

$$\begin{aligned} A_{oj} &= t_o t_j - b_o b_j & B_{oj} &= t_o b_j + t_j b_o \\ C_{ij} &= x_{2j-1} - x_i & D_{ij} &= x_{2j} - x_i \\ E_{ij} &= D_{ij}^2 + z_j^2 & F_{ij} &= C_{ij}^2 + z_j^2 \\ t_j &= \cos I_j \cos D_j & b_j &= \sin I_j \end{aligned} \quad (2)$$

where t_j and b_j are the direction cosines linked with the magnetization vector of the source body, t_o and b_o represent the direction cosines of the geomagnetic field vector, I_j and D_j are the inclination and declination of the field, respectively, and T_0 denotes the datum level (Leite and Leao, 1985). Equation 1 was used here to produce a total field magnetic anomaly of a vertical prismatic block with a bottom at infinity. Based on the superposition principle, twice the evaluation of this equation for two different depth levels and the subtraction of these two calculations provides the anomaly of a vertical prismatic block with a top and a finite bottom.

The total field magnetic anomaly of a volume of magnetized material over the region R is calculated approximately by the following definition (Blakely, 1996)

$$\Delta T = -C_m \hat{F} \cdot \nabla_P \int_R M \cdot \nabla_Q \frac{1}{r} dv, \quad (3)$$

where M denotes the magnetization, the distance between the observation point P and the element dv of the source is represented by r , Q is the position of dv , F represents the unit vector in the regional field direction, and C_m is the balancing operator which depends on the system in use. If this definition is modified for a 3D rectangular prism with infinite depth extent which is placed parallel to the axes of the 3D Cartesian coordinate system, the following definition provides the total field magnetic anomaly at the origin (Bhattacharyya 1964; Blakely, 1996)

$$\begin{aligned} \Delta T = C_m M & \left[\frac{\alpha_{23}}{2} \log\left(\frac{r-x'}{r+x'}\right) + \frac{\alpha_{13}}{2} \log\left(\frac{r-y'}{r+y'}\right) \right. \\ & - \alpha_{12} \log(r+z_1) - \hat{M}_x \hat{F}_x \arctan\left(\frac{x'y'}{x'^2+r z_1+z_1^2}\right) \\ & \left. - \hat{M}_y \hat{F}_y \arctan\left(\frac{x'y'}{r^2+r z_1+x'^2}\right) + \hat{M}_z \hat{F}_z \arctan\left(\frac{x'y'}{r z_1}\right) \right] \end{aligned} \quad (4)$$

$$\begin{cases} x' = x_2 \\ x' = x_1 \end{cases} \begin{cases} y' = y_2 \\ y' = y_1 \end{cases}$$

where

$$\begin{aligned}\alpha_{12} &= \hat{M}_x \hat{F}_y + \hat{M}_y \hat{F}_x & \alpha_{13} &= \hat{M}_x \hat{F}_z + \hat{M}_z \hat{F}_x \\ \alpha_{23} &= \hat{M}_y \hat{F}_z + \hat{M}_z \hat{F}_y & r^2 &= x^2 + y^2 + z^2\end{aligned}\quad (5)$$

Here, Equation 4 was used to produce a total field magnetic sign of rectangular prism with a bottom at infinity. Again, based on the superposition principle, the magnetic anomaly due to a 3D rectangular prism with a top and a finite bottom is obtained. A more detailed definition for this equation can be found in Blakely (1996).

3. Synthetic and real data applications

In the synthetically produced applications, both nonmagnetized and magnetized host mediums were used. Using Equations 1 and 4 theoretical aeromagnetic anomalies were obtained with 0.5 km data sampling intervals. Directions of the magnetization and ambient field were set to be parallel to each other in the computations. The inclination and the declination of the Earth's magnetic field were assigned as 55° and 0°, respectively. In the real data example, aeromagnetic anomalies of the Mount Nemrut stratovolcano which has an uneven rugged topography were used. The aeromagnetic data set was acquired by General Directorate of Mineral Research and Exploration of Turkey (MTA) with profile intervals of 1–2 km using 70 m sampling rates along with the profiles. Flight height of 2000 feet (~610 m) from the ground surface was used in the drape flying mode. Except for the IGRF correction, all others were performed by MTA. Here, the algorithm of Baldwin and Langel (1993) was used for this correction. In both synthetic and real field anomaly cases reduced-to-the-pole (RTP) anomalies were calculated using the following definition (Blakely, 1996)

$$\Delta T_{RTP} = F^{-1} \left[\Psi_{RTP} F(\Delta T) \right], \quad (6)$$

where ΔT_{RTP} is the RTP anomaly, F and F^{-1} represent the Fourier and inverse Fourier transforms, Ψ_{RTP} and ΔT are the RTP filter in the wavenumber domain and the observed magnetic anomaly, respectively. In every experiment, the lengths of the profile and grid data sets were increased to the next higher power of 2, and the added data bands were removed at the end of the RTP process to eliminate the edge effects that occurred due to the nature of the fast Fourier transform. Additionally, in order to follow the abrupt lateral changes in the magnetization, total horizontal derivatives (THD) of the synthetic and real magnetic anomalies were obtained through a simple finite difference approach using the following expression (Blakely, 1996)

$$THD = \left[\left(\frac{\partial \Delta T}{\partial x} \right)^2 + \left(\frac{\partial \Delta T}{\partial y} \right)^2 \right]^{1/2}, \quad (7)$$

where ∂x and ∂y represent the horizontal derivatives along two directions in the map space.

3.1. Synthetic examples

3.1.1. Nonmagnetized host medium

In the first synthetic example, equally-spaced three source bodies were used. A gentle sloping nonmagnetized host medium covers these source bodies. The synthetic topography has a slope of 4% which likely covers the most real field situations. Causative bodies have an intensity of magnetization of 0.1 A/m and the constant regional (CR) value is 20 nT. 2D plan views of the bodies and the covering host medium are illustrated in Figure 1. The aeromagnetic signs of the 2D and 3D source bodies and their RTP and THD anomalies are shown in the same figure. Although they have the same physical properties (thickness, width and intensity of magnetization), the first body generates the highest RTP anomaly amplitude (red solid line) in the drape flying aeromagnetic survey mode due to the topographical change along with the surveying path. As expected, increasing source depths along the profile give rise to the lowering of the anomaly amplitudes for the other bodies. The same finding is clearly observed in the 3D case. However, since the host medium is nonmagnetized level flying mode using a constant elevation of 5 km above sea level produces exactly the same RTP anomaly responses for three source bodies. The THD image maps also show that the same amplitude maximum horizontal gradients are observed over the source bodies in the level flying mode. As it is well known, the distance between the magnetized sources and the measurement plane significantly affects the magnetic anomaly amplitudes. In this example, although these three causative structures have the same physical parameters such as thickness, shape and intensity of magnetization, they produce different anomaly amplitudes in the drape flying mode due to the topography of the host medium. On the other hand, level flying mode eliminates this effect. It must be noted that if a comparison about these buried source structures is made by considering only the anomaly amplitudes obtained through the drape flying mode, it can be thought that these structures have different physical properties. Hence level flying is seemed to be more preferable surveying mode in such topographic cases when the host medium is nonmagnetized or has an ignorable magnetization.

In the second example of nonmagnetized host medium case, an uneven synthetic topography having a maximum slope of about 15% along the surveying path was considered. This slope rate is reasonable for helicopter-borne surveying systems (Coyle et al., 2014). Source bodies which are shown in Figure 2 have different intensities of magnetization ranging between 0.1 and 0.25 A/m in this case. The ambient field has a CR of 20 nT. The effects of the topographic changes along the profile are clearly observed in the drape flying mode. Although the buried two source

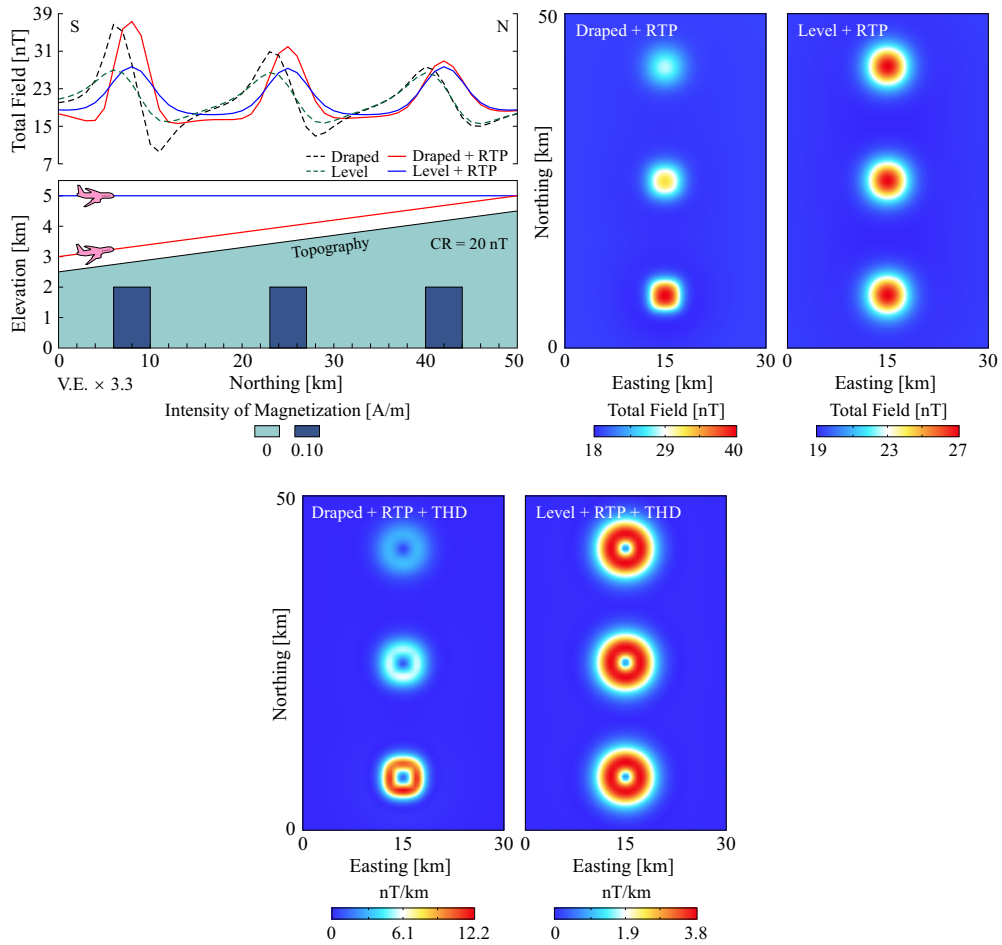


Figure 1. Synthetic aeromagnetic anomalies calculated at constant altitude above sea level and at a drape surface. Image maps show the responses of 3D causative bodies. Nonmagnetized host medium having a gently sloping topography was used in both 2D and 3D cases.

bodies having the magnetization intensities of 0.1 and 0.12 A/m produce maximum RTP anomaly amplitudes that are very close to each other in level flying survey mode, the maximum anomaly amplitude of the first one is quite higher than the latter one in the drape flying mode due to the distance between observation surface and the source depths. On the other hand, the RTP response of the source body having the magnetization intensity of 0.18 A/m is more evident in the drape flying mode. Insignificant anomaly response for this body is observed in the level flying mode. The same case is also seen for the source bodies which have the magnetization intensities of 0.2 and 0.25 A/m. The image maps showing the magnetic responses of 3D bodies also exhibit the same RTP anomaly patterns as in the 2D case. The weak aeromagnetic anomaly amplitudes arising from the small masses are more evident in the drape flying mode. However, a smoother anomaly patterns are observed in the level flying mode without any abrupt lateral changes in the amplitudes. The remarkable

topographic change just above the causative body located nearly at the end of the survey profile distorts the shape of the aeromagnetic sign in the drape flying mode. This distortion is not observed in the level flying mode. The THD image maps (Figure 2) show that the edges of the source bodies are better resolved in drape flying mode. The edges of the source body which has the magnetization intensity of 0.18 A/m could not be determined in the level flying mode. THD operator could not produce sharpened amplitude responses at the edges of source bodies in this flying mode. This instance clearly demonstrates that both flying modes have some advantages over each other depending on the source body positions in the subsurface and the topographic changes of the investigated area.

3.1.2. Magnetized host medium

Two different scenarios including moderately and strongly magnetized earth models were used in the magnetized host medium case. Magnetization and ambient field directions are parallel to each other as mentioned previously. The

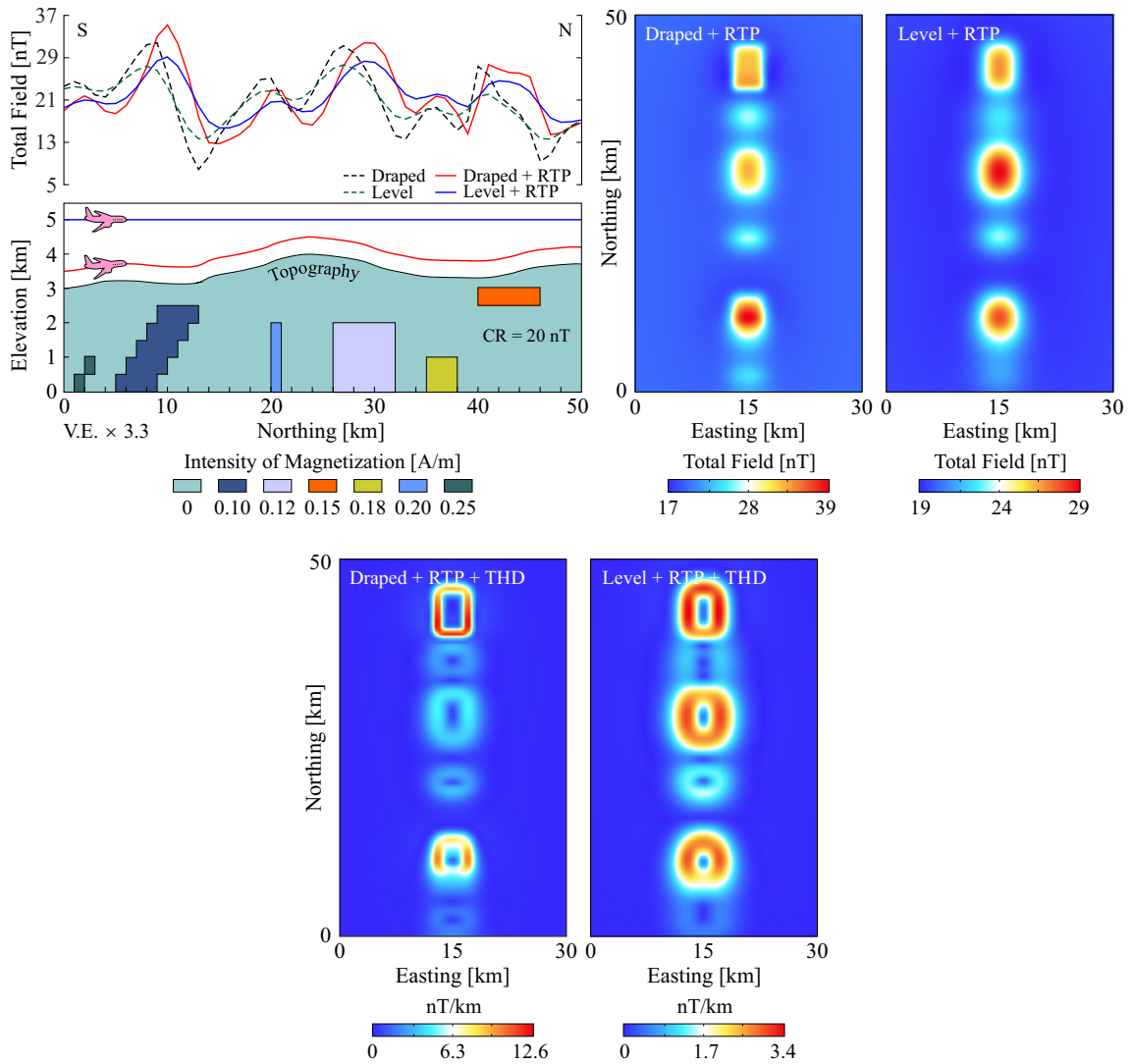


Figure 2. Synthetic aeromagnetic anomalies calculated at constant altitude above sea level and at a drape surface. Image maps show the responses of 3D causative bodies. Nonmagnetized host medium having a rugged topography was used in both 2D and 3D cases.

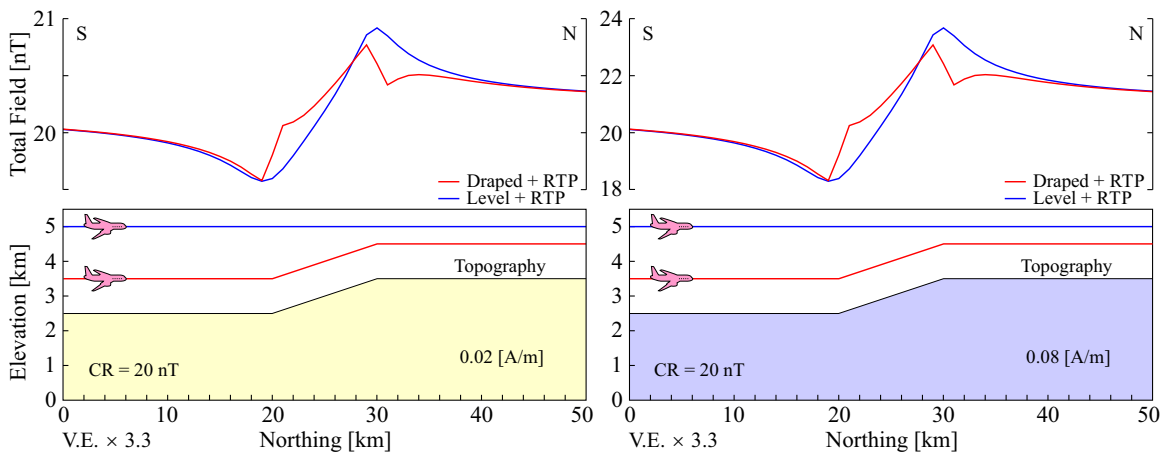


Figure 3. Magnetic responses of moderately and strongly magnetized host mediums. Magnetization intensities of the host mediums are shown in each plot.

synthetic topography has flat surfaces of different heights at the beginning and end of the surveying path, while it has a slope of 10% in the middle parts. CR is 20 nT in both experiments. The host mediums and their aeromagnetic anomalies are illustrated in Figure 3. The amplitude of the magnetic signal originated from the earth model having a higher intensity of magnetization is larger as expected. The distortions at the beginning and end of the sloping topography are clearly seen in aeromagnetic anomalies obtained via drape flying mode. These effects are not seen in the magnetic responses of level flying mode case. It must be noted that if the flight height of the draped mode is increased these effects will decrease or vice versa. Three causative bodies which have the same intensity of magnetization (0.1 A/m) are positioned in both earth models. The last body along with the profile is thicker than the other ones. Figure 4 shows the aeromagnetic anomalies of 2D and 3D sources and the plan views of the sources.

THD anomalies of the RTP responses are also shown. In the drape flying survey mode, the RTP magnetic response of the buried source closest to the beginning of the profile is the highest. The sudden topographic increase causes the structure which is positioned in the middle part of the profile to produce a lower RTP anomaly in this flying mode. Additionally, it is clearly seen that the thickest model body does not produce the highest RTP amplitude due to the distance to the observation height. On the other hand, the thickest body produces the highest anomaly while the same amplitude anomalies arise from the first two ones in the level flying mode. This finding indicates that the level flying mode is more advantageous in such cases. It must be also noted that although the effects of the sudden topographic changes in the middle parts of the surveying profile are not clearly observed in RTP image maps, these undesired terrain effects are noticeable in the THD anomalies in both flying modes (Figure 4).

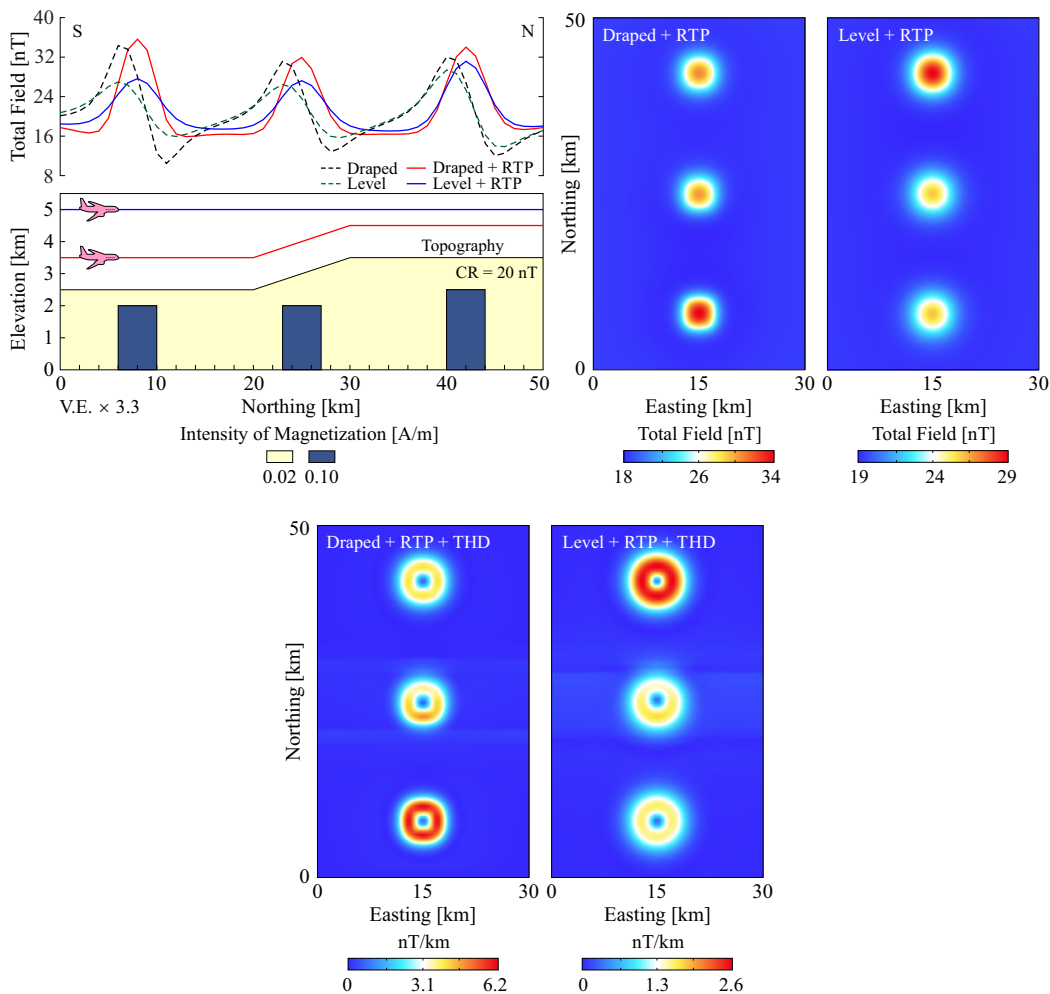


Figure 4. Synthetic aeromagnetic anomalies calculated at constant altitude above sea level and at a drape surface. Image maps show the responses of 3D causative bodies. Moderately magnetized host medium having an abrupt change in slope was used in both 2D and 3D cases.

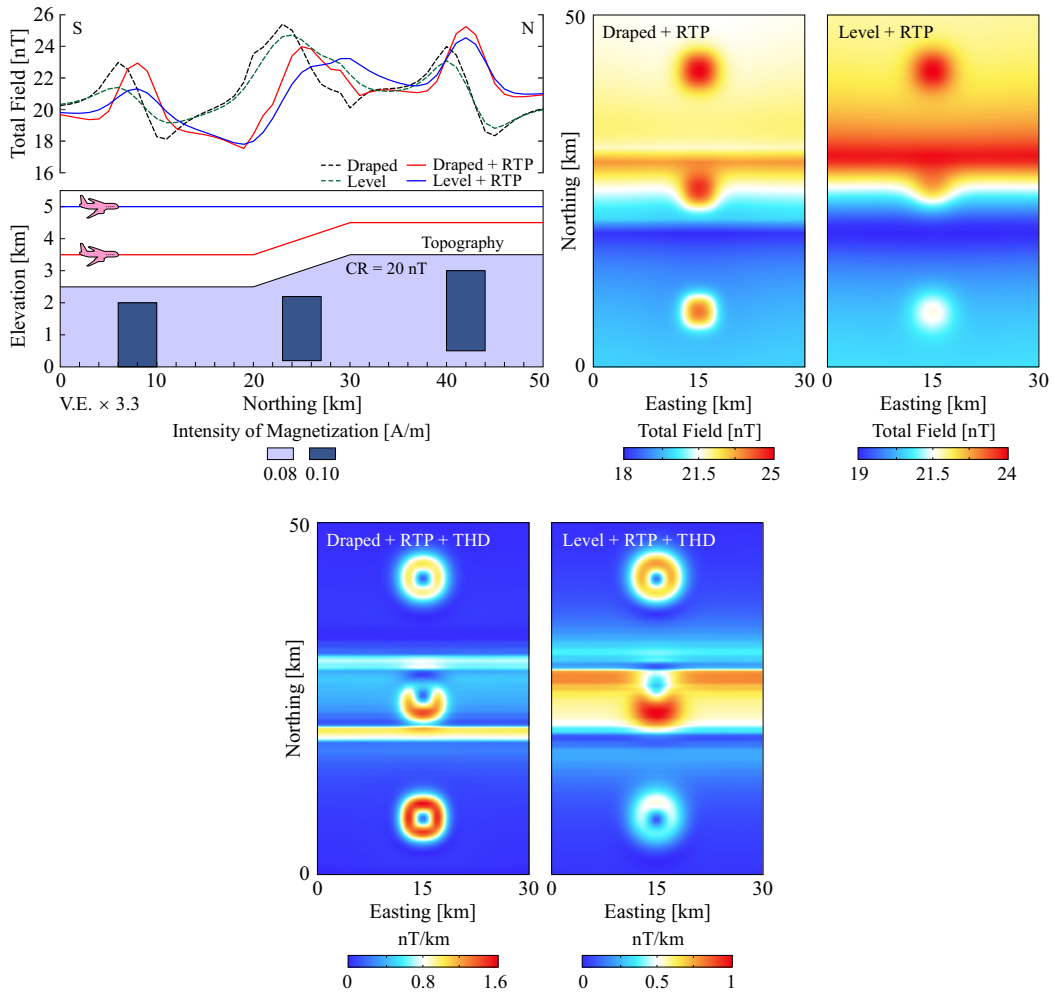


Figure 5. Synthetic aeromagnetic anomalies calculated at constant altitude above sea level and at a drape surface. Image maps show the responses of 3D causative bodies. Strongly magnetized host medium having an abrupt change in slope was used in both 2D and 3D cases.

In the second example of the magnetized host medium case, the magnetization intensity of the host medium was increased considerably, namely 4 times compared to the previous example to better understand the effects of strongly magnetized terrains on the aeromagnetic anomalies. Additionally, the depths to the top of the source bodies were adjusted to match the changes in the surface topography and the flight height of the drape flying mode. The aeromagnetic simulations of this case and the plan views of the source bodies are shown in Figure 5. THD image maps obtained from RTP anomalies are also demonstrated. In this example, some findings appear to be complicated because of the strongly magnetized host medium. In the drape flying mode, as seen in the 2D plot, the RTP anomaly of the body that is located in the middle part of the profile has a maximum amplitude over the source. However, the maxima occurred due to the abrupt topographic change located 30 km from the beginning of

the profile mask the maximum RTP anomaly of the source body in the level flying mode. Accordingly, a lateral shift in the magnetic high is clearly observed in this flying mode. This distortion in the anomaly amplitudes may cause misinterpretation about the location of the source body. In the RTP magnetic responses, since the flight heights are close to each other, no remarkable amplitude changes arise from the thickest body for two flying modes. However, the difference between the amplitudes is quite observable for the causative source located at the beginning of the profile due to the distance between two observation heights. In the RTP image maps (Figure 5) the effects of the topographical changes are more evident. If the topographic effects are not taken into consideration in the drape flying survey mode, the abrupt lateral anomaly amplitude changes in the RTP image map seem as if they represent the contacts of different geological units or faults cutting the survey area transversely. These topographic

effects which are occurred due to the strongly magnetized host medium is observed in a smoother form in level flying survey mode, which provides an advantage. On the other hand, because of the increased height in the level flying mode the RTP anomaly of the first body is weaker. Additionally, the RTP image map in Figure 5 shows that maximum amplitudes are not observed over the source body located at the middle parts of the profile. THD image maps show that derivative-based techniques are highly sensitive to significant topographic changes in strongly magnetized host mediums. Additionally, the edges of the source body that is located in the middle part of the grid plane could not be resolved (Figure 5). The simulations performed here with synthetic data sets indicate that both flying modes have some advantages and disadvantages over each other. Besides the amplitudes of the magnetic terrain effects should not be ignored in case of strongly magnetized host mediums having uneven topographies.

3.1.3. Data continuation between arbitrary surfaces

An analytic continuation process transforms the potential field anomaly observed on a surface to the field that would be observed on another surface. This new surface can be farther or closer from all sources. The following expression (Blakely 1995) is used for the computation

$$\Delta T_{Con} = F^{-1} \left[e^{-\Delta z |k|} F(\Delta T) \right], \quad (8)$$

where ΔT_{Con} represents the analytically continued data, e is the exponential function, Δz denotes the continuation height, $|k|$ represents the radial wavenumber at grid points throughout the k_x and k_y plane and is obtained as given below

$$|k| = \left(k_x^2 + k_y^2 \right)^{1/2}. \quad (9)$$

There is a significant issue for this computation. Since standard wavenumber domain Fourier filtering techniques allow data reduction or continuation from only one level surface to another level surface (Nabighian et al., 2005), this process cannot be performed between arbitrary/uneven surfaces using standard wavenumber domain techniques. Therefore, Schwarz–Christoffel transformation (Parker and Klitgord, 1972), extended potential field theory (Syberg, 1972; Hansen and Miyazaki, 1984), chessboard technique (Cordel, 1985), Taylor series expansion (e.g., Cordell and Grauch, 1985; Pilkington and Thurston, 2001) and equivalent source technique (e.g., Mendonça and Silva, 1994, 1995) are generally used for this procedure. Ridsdill-Smith and Dentith (2000) suggested a wavelet transform technique for the drape corrections. To the best of my knowledge, the most commonly used technique is the chessboard technique of Cordel (1985) in which the potential field is calculated at sequentially higher levels followed by interpolation

between several levels, and analytic continuation using a Taylor series expansion. Moreover, a computational extension (Paterson et al., 1990) integrated into a widely used commercial software suite (Oasis Montaj) applies the technique of Cordel (1985), and draped data can be transformed to a potential field on a new surface of a predetermined height, namely level data. But a simple usage strategy for Equation 8 can be performed for the desired transformation. That is, analytical continuation from a constant horizontal plane to an uneven surface or vice versa can be achieved by the repeated evaluations of the Equation 8 to the grid for each grid point with its own continuation distance. In each time, the new magnetic value of each grid point is stored. In this way, every magnetic value can be reduced to a horizontal plane or a draped surface through different continuation heights for each data point. To examine the validity and reliability of the proposed technique aeromagnetic responses of three synthetic model bodies were used. These models bodies which have the same bottom depths (3 km below sea level) were assumed to be located below a rugged synthetic topography. The elevations of the observation points are in the range of between 0.75 km and 2.95 km above sea level. Same as the previous examples 20 nT was used for CR. The thicknesses and magnetization intensities of the bodies were set as 2 km and 0.1 A/m, respectively. In order not to isolate topographic effects and magnetic anomalies the produced synthetic data were not contaminated with a noise content. The positions of the model bodies and the considered synthetic topography are shown in Figure 6a. The 3D forward modeling procedure was performed using a drape flying mode with a constant terrain clearance of 1 km above the ground surface. Figure 6b illustrates the RTP anomaly of the draped data. The effects of the topographic changes on the shapes and the amplitudes of the magnetic signs are observable. The northernmost anomaly has the highest amplitudes as expected. However, although the source body which is located in the middle parts of the grid plane is larger in size, the southernmost source body produces a higher amplitude RTP response. This finding clearly reveals the effects of the surface topography on the anomaly amplitudes. Figures 6c and 6d show the RTP anomalies obtained through the chessboard technique and the proposed computational procedure, respectively. In both techniques, every single magnetic observation value was one by one reduced to a horizontal plane corresponding over the highest observation point, namely 3.95 km above sea level. The aeromagnetic response of the southernmost source body is the lowest in each anomaly map, as it should be. Both techniques produce almost the same anomaly patterns. However, a detailed look shows that the innermost contour line of the northernmost body is more circular in Figure 6d, but both theoretically and practically this inconsiderable change should not be

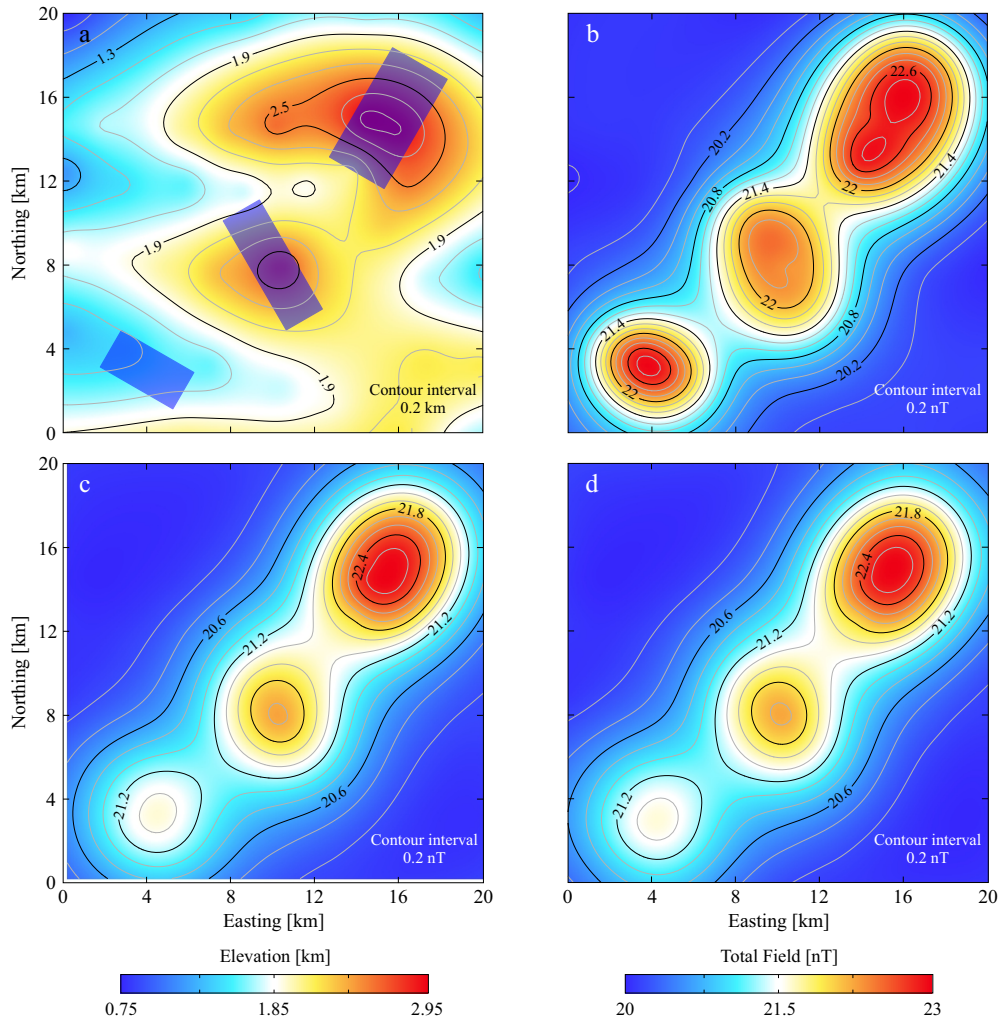


Figure 6. a) Synthetic topography and the locations of the causative bodies, b) Magnetic anomalies of the causative bodies calculated 1 km above ground surface, c) Magnetic anomalies reduced to a horizontal datum plane coinciding the highest observation point through the chessboard technique, d) Magnetic anomalies reduced to a horizontal datum plane coinciding the highest observation point through the suggested computational procedure.

a complication. These reduced data image maps indicate that suggested computational procedure produces results at least as successful as the commonly used chessboard technique.

3.2. Real data example

Mount Nemrut stratovolcano which is known as the youngest volcanic center in eastern Turkey has situated nearby the southwestern coast of Lake Van (Figure 7). The volcanism in the country is associated with the tectonic regime of the region, namely the collision between the Anatolian and Arabian plates (Yılmaz et al., 1998; Karaoğlu et al., 2004; Özdemir et al., 2006). Nearly 25 % of the country's area is covered by volcanics. The polygenetic stratovolcano (Yılmaz et al., 1998) has a large natural relic

summit caldera (Seven et al., 2019) and two permanent (Nemrut and Hot lakes) and three seasonal small lakes. Lake Nemrut is filled with fresh water and has a maximum depth of 176 m while the Hot Lake has a maximum depth of about 11 m (Ulusoy et al., 2008). Most of the other parts of the collapsed Nemrut caldera are covered by some maar deposits, domes and lava flow. The geological map of the Nemrut stratovolcano and its close vicinity is shown in Figure 7. The spectacular summit caldera has diameters of about 8.5×7 km (Ulusoy, 2008) and it has a wall of about 688 m high (Yılmaz et al., 1998). The highest part of the Nemrut caldera rim is the Sivri hill and it is about 2935 m high (Yılmaz et al., 1998; Ulusoy et al., 2008). The nearly elliptical-shaped Nemrut stratovolcano covers an area of about 486 km² (27 km \times 18 km) (Yılmaz et al., 1998). The

the presence of a magma chamber at the depths of about 4–5 km (Ulusoy, 2008). A recent study (Ekinçi et al., 2020) which supports the finding of the magma chamber, reported the first detailed geophysical investigation of the stratovolcano and its surrounding.

The rugged terrain in the region (Figure 7) provides a good opportunity for investigating the aeromagnetic data reduction process and terrain effects. Hence, aeromagnetic anomalies having a resolution of 1 km × 1 km grid interval were used. As mentioned previously the aeromagnetic anomalies were obtained by MTA using a flight height of 2000 feet (~610 m) from the surface topography using drape flying mode. The RTP image map of the draped data is presented in Figure 8a. High magnetic anomalies located north and west of the caldera rim (black circle) are evident. To make a comparison every single aeromagnetic observation was continued to the highest observation height. Here, taking into account the flight height and the highest point of the stratovolcano (about 2935 m above sea level) the aeromagnetic data were reduced to a horizontal datum plane which has an elevation of 3500 m above sea level. The RTP image map of the reduced data is exhibited in Figure 8b. Although this process resulted in a loss of short wavelength anomalies, namely smoother form, the main magnetic highs still exist on north and east of the caldera. These high amplitude signs are probably originated from Kantaşı ignimbrite shown in Figure 7. Moreover, comendite and basaltic flows (Figure 7) associated with the bimodal rift activity between Kantaşı hill and Nemrut plain contribute to the increasing of the anomaly amplitudes in that region. On the other hand, since there has not been such an activity Nemrut ignimbrite does not produce such magnetic highs. Magnetic response of the trachyte, the product of the pre-caldera stage of the volcanism, is seen in the wider area. This case may point out the extension of the trachyte towards the west beneath the Nemrut ignimbrite. To follow abrupt lateral changes in the magnetization THD anomaly maps of RTP applied draped and level data are shown in Figures 8c and 8d, respectively. Poorly resolved amplitudes are traced in Figure 8c. Significant anomaly responses are not observed in the vicinity of the caldera. Additionally, no noteworthy high amplitude anomalies indicate abrupt lateral changes in the magnetization in the other parts of the study area. However, the steepest horizontal gradients of the pole reduced level data are more improved (Figure 8d). The contacts of Nemrut and Kantaşı ignimbrites located north of the caldera rim are well resolved. Some moderate THD anomalies are seen in the contacts of the ignimbrites in other parts of the study area. To the west of the caldera, the contact of the trachyte produces high THD signs. In the vicinity of the Nemrut rift zone, high amplitudes are also observed. According to these findings, it is seen

that the level data produce more compatible results with the geological map of the study area. In the next step, another edge determining algorithm, namely THD of the tilt angle (TA) which uses more derivative operator was used. TA operator is the generalized local phase which has a range of -90° to $+90^\circ$ from the horizontal (Miller and Singh, 1994). The procedure produces positive amplitudes over the sources, and zero over the edges. The following definition is used for the computation of TA amplitudes

$$TA = \tan^{-1} \frac{\left[\frac{\partial \Delta T}{\partial z} \right]}{\left[\left(\frac{\partial \Delta T}{\partial x} \right)^2 + \left(\frac{\partial \Delta T}{\partial y} \right)^2 \right]^{1/2}}, \quad (10)$$

where ∂z is the vertical derivative. Here, vertical derivative amplitudes were calculated using the equation given below (Blakely, 1996)

$$\Delta T_{ver} = F^{-1} \left[|k| F(\Delta T) \right]. \quad (11)$$

TA operator is easier to interpret than the analytic signal phase angle (Cooper and Cowan, 2006) and it remarkably improves weak potential field anomalies. THD of the TA is suggested for sharpening the source edges and enhancing the subtle details in the potential field anomaly maps (Verduzco et al., 2004). Figure 8e shows the response of this operator using the draped data. The map is dominated by both low and high amplitude responses. There is no correlation between these amplitudes and the geologic and topographic properties of the study area. Additionally, using much more derivative operators makes the response map noisier (Figure 8e) than does the conventional THD operator (Figure 8c). Hence, it can be mentioned that aeromagnetic anomalies acquired through drape flying mode over rugged magnetized terrains are not suitable for grid operators which use more derivative operations. It must be also noted that grid operations performed in the wavenumber domain are more suitable for level data sets than draped data sets as mentioned previously. The THD map of the TA of the pole reduced level data is shown in Figure 8f. Some anomaly patterns can be observed in the image map. High amplitude signs of the subtle details can be tracked easily. However, when considering the topographical map (Figure 7) of the studied region it is seen that derivative-based operator responds to the edges of the high reliefs. Higher anomaly amplitudes are originated from the rim of the Nemrut caldera, Mazik, and Kirkor domes which are shown in Figure 7. Additionally, Bitlis metamorphics having sharp and high reliefs located on the southernmost of the study area produce high amplitude patterns (Figure 8f). It is observed that these terrain-induced effects are not disappeared even though

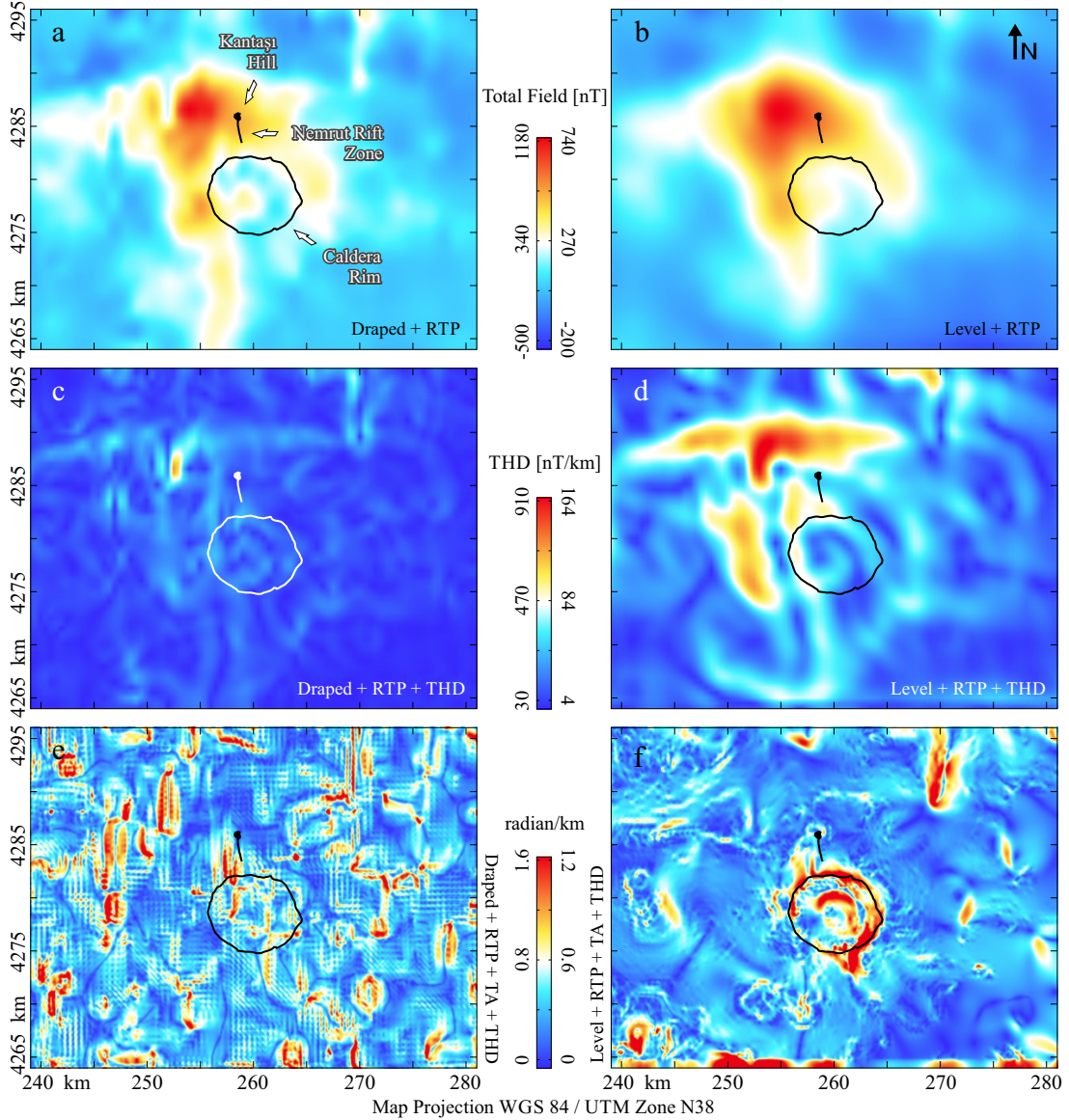


Figure 8. a) RTP applied aeromagnetic anomalies of the Mount Nemrut stratovolcano observed about 610 m above the ground surface, b) Level data of the anomaly shown in panel a. The anomalies were reduced to a horizontal datum plane 3500 m above sea level c) THD map of the anomaly shown in panel a, d) THD map of the anomaly shown in panel b, e) THD map of TA of the anomaly shown in a, f) THD map of TA of the anomaly shown in b.

they do not attract much attention in the aeromagnetic anomaly maps shown in Figures 8a and 8b. In the last step, pseudogravity (PSG) transformation which attenuates the short wavelength anomalies was applied to aeromagnetic data sets using the following definition (Blakely, 1996)

$$\Delta T_{PSG} = F^{-1} \left[\Psi_{PSG} F(\Delta T) \right], \quad (12)$$

where ΔT_{PSG} is the PSG anomaly and Ψ_{PSG} is the PSG filter in the wavenumber domain. Figures 9a and 9b show the PSG anomalies of the draped and level aeromagnetic data

sets, respectively. A smoother anomaly pattern is observed for the level data. The contacts of the Nemrut and Kantaşı ignimbrites located north of the caldera rim and the steepest horizontal gradients located at the other parts of the study area are resolved partially in both THD maps (Figures 9c and 9d). Additionally, these anomaly signs are weak in draped mode (Figure 9c) and spread over a wider area than it should be in the level mode (Figure 9d). Furthermore, similar to the previous one, using much more directional derivative operators could not produce

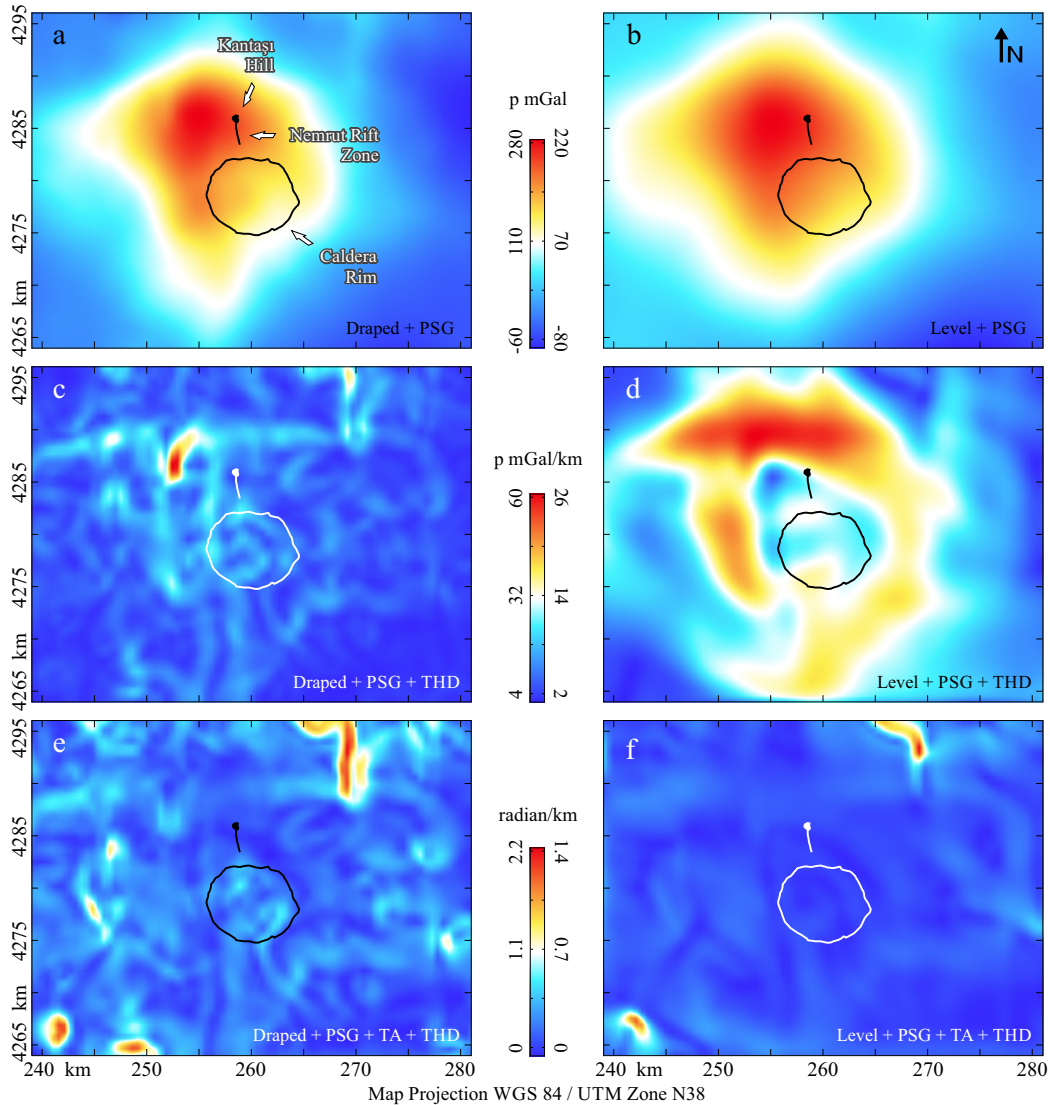


Figure 9. a) PSG anomalies of the draped aeromagnetic data set, b) Level PSG data of the anomaly shown in panel a. The anomalies were reduced to a horizontal datum plane 3500 m above sea level c) THD map of the anomaly shown in panel a, d) THD map of the anomaly shown in panel b, e) THD map of TA of the anomaly shown in a, f) THD map of TA of the anomaly shown in b.

satisfactory solutions for draped (Figure 9e) and level PSG (Figure 9f) data sets.

4. Conclusion

In the aeromagnetic surveys, data acquisition is performed using either a constant terrain clearance in which the distance is the same above the ground surface or a constant elevation above sea level. The first one is called drape flying mode while the latter one is a level flying mode. Here, possible effects of both flying survey modes on the aeromagnetic anomalies were investigated using theoretical and real data sets. In the theoretical examples,

nonmagnetized and magnetized host mediums were considered using 2D and 3D hypothetical subsurface causative bodies. Additionally, magnetic terrain effects were also examined. In the real data example, aeromagnetic data of the Mount Nemrut stratovolcano (Bitlis, Eastern Turkey) acquired using a drape flying mode were analyzed. The sharp and rugged topography of the studied region was an important factor in the selection of this aeromagnetic data set.

Theoretical and real data experiments showed that drape and level flying modes have some advantages and shortcomings over each other. In the case of significant

topographical changes amplitudes of draped and level anomalies quite differ from each other. In the level flying mode nearly the same causative bodies cause magnetic signs of similar amplitude on the anomaly map and they can be compared easily. However, the remarkable loss of resolution of small-sized anomaly sources can arise when the flight elevation is high. Drape flying mode is more sensitive to terrain effects, and rapid topographic changes in rugged terrains may cause too severe spurious phases in the aeromagnetic anomalies. On the other hand, it can be mentioned that inconspicuous terrain-induced effects are present even in the level data anomalies in the areas having strongly magnetized rugged topographies and they can be enhanced when applying grid operations which have much more directional derivative operators. Therefore, as clearly seen from the real data example presented here, edge approximating algorithms using too many directional derivative operators are not recommended for the aeromagnetic anomalies obtained over the regions of rugged high topographic reliefs to avoid misinterpretation.

Although grid operations performed in the wavenumber domain are commonly used for draped aeromagnetic data, they are suitable for level data acquired over a horizontal plane, and some modifications are needed for draped data. Hence, the data acquired using drape flying mode must be reduced to a horizontal datum plane, namely level data. This plane should coincide over the highest topography and the observation height. To that end, the validity of an easy computational procedure for the data reduction

was also presented. Even though the repeated use of fast Fourier Transform (i.e. \times number of the data points in the grid) seems to require large computational time, examples presented here showed that computation time is not more than 48 s for a data set having a grid size of 128×128 through a laptop having 2.80 GHz processor with a memory of 16.0 GB. It must be also noted that the software package mentioned previously allow a continuation of loose drape surveys to a tight drape or transformation of drape flown surveys to barometric level flown surveys. However, there is no possibility for the reduction of the aeromagnetic data of level flown survey acquired over a constant height above sea level to an uneven draped surface. On the other hand, this data reduction can be easily achieved through the computational procedure presented here if the draped surface is higher than the level height. If not, the suggested technique can be also performed with the help of some advanced approaches which prevent the possible undesired effects that can be occurred due to the unstable nature of the downward continuation.

Acknowledgments

Thanks are due to Prof. Dr. Mümtaz Hisarlı (İstanbul University) for constructive review that greatly improved the paper. Other three anonymous reviewers are also thanked for their suggestions. The aeromagnetic data set used here was obtained from MTA through a project (Project No: BEBAP 2018.04) supported by the Scientific Research Projects Foundation of Bitlis Eren University (Turkey).

References

- Aydar E, Gourgaud A, Ulusoy İ, Digonnet F, Labazuy P et al. (2003). Morphological analysis of active Mount Nemrut stratovolcano, eastern Turkey: evidences and possible impact areas of future eruption. *Journal of Volcanology and Geothermal Research* 123: 301-312.
- Baldwin RT, Langel RA (1993). Tables and Maps of the DGRF 1985 and IGRF 1990. *IAGA Bulletin* 54: 158.
- Bhattacharyya BK (1964). Magnetic anomalies due to prism-shaped bodies with arbitrary polarization. *Geophysics* 29: 517-531.
- Blakely RJ (1996). *Potential Theory in Gravity and Magnetic Applications*. Cambridge, UK: Cambridge University Press.
- Cooper GRJ, Cowan DR (2006). Enhancing potential field data using filters based on the local phase. *Computers & Geosciences* 32: 1585-1591.
- Cordell L (1985). Applications and problems of analytical continuation of New Mexico aeromagnetic data between arbitrary surfaces of very high relief. In: *Proceedings of the International Meeting on Potential Fields in Rugged Topography*. Lausanne, Switzerland: Institute of Geophysics, University of Lausanne, pp. 96-101.
- Cordell L, Grauch VJS (1985). Mapping basement magnetization zones from aeromagnetic data in the San Juan Basin, New Mexico. In: Hinze WJ (editor). *Utility of Regional Gravity and Magnetic Maps*. Tulsa, OK, USA: Society of Exploration Geophysicists (SEG), pp. 181-197.
- Coyle M, Dumont R, Keating P, Kiss F, Miles W (2014). Geological Survey of Canada aeromagnetic surveys: design, quality assurance, and data dissemination. *Geological Survey of Canada, Open File 7660*. doi: 10.4095/295088
- Çubukçu HE (2008). Petrologic evolution of Nemrut Stratovolcano (Turkey): Peralkaline magmatism in a collisional domain. PhD, Hacettepe University, Ankara, Turkey.
- Ekinci YL (2010). A Matlab-based interactive data processing and interpretation software package for gravity and magnetic anomalies: GMINTERP. In: *19th International Geophysical Congress and Exhibition*; Ankara, Turkey. pp. 1-4.
- Ekinci YL, Yiğitbaş E (2012). A geophysical approach to the igneous rocks in the Biga Peninsula (NW Turkey) based on airborne magnetic anomalies: geological implications. *Geodinamica Acta* 25: 267-285.

- Ekinci YL, Yiğitbaş E (2015). Interpretation of gravity anomalies to delineate some structural features of Biga and Gelibolu peninsulas, and their surroundings (north-west Turkey). *Geodinamica Acta* 27: 300-319.
- Ekinci YL, Büyüksaraç A, Bektaş Ö, Ertekin C (2020). Geophysical investigation of Mount Nemrut stratovolcano (Bitlis, Eastern Turkey) through aeromagnetic anomaly analyses. *Pure and Applied Geophysics* 177: 3243-3264.
- Hansen RO, Miyazaki Y (1984). Continuation of potential fields between arbitrary surfaces. *Geophysics* 49: 787-795.
- Hildenbrand TG, Raines GL (1987). Need for aeromagnetic data and a national airborne geophysics program. In: *Proceedings of the U.S. Geological Survey Workshop on Geological Applications of Modern Aeromagnetic Surveys; Colorado, USA*. pp. 1-6.
- Hinze WJ, von Frese RRB, Saad AH (2013). *Gravity and Magnetic Exploration: Principles, Practices and Applications*. Cambridge, UK: Cambridge University Press.
- Grauch VJS, Campbell DL (1984). Does draping aeromagnetic data reduce terrain-induced effects? *Geophysics* 49 (1): 75-80.
- Güner Y (1984). *Doğu Anadolu Kuvaterner Volkanizması (Nemrut Yanardağı)*. Ankara, Turkey: MTA Genel Müdürlüğü, Temel Araştırmalar Dairesi, p. 77.
- Karakhanian A, Djrashian R, Trifonov V, Philip H, Arakelian S et al. (2002). Holocene-historical volcanism and active faults as natural risk factors for Armenia and adjacent countries. *Journal of Volcanology and Geothermal Research* 113: 319-344.
- Karaoğlu Ö, Özdemir Y, Tolluoğlu AÜ (2004). Physical evolution, emplacement of ignimbrite and characteristic eruption types of Nemrut Stratovolcano: a caldera system at Eastern Anatolia-Turkey. In: *Proceedings of the 5th International Symposium on Eastern Mediterranean Geology; Thessaloniki, Greece*. pp. 1287-1290.
- Karaoğlu Ö, Özdemir Y, Tolluoğlu AÜ, Karabıykoğlu M, Köse O et al. (2005). Stratigraphy of the volcanic products around Nemrut caldera: implications for reconstruction of the caldera formation. *Turkish Journal of Earth Sciences* 14: 123-143.
- Karaoğlu Ö, Elshaafi A, Salah MK, Browning J, Gudmundsson A (2017). Large-volume lava flows fed by a deep magmatic reservoir at Ağrı Dağı (Ararat) volcano, Eastern Turkey. *Bulletin of Volcanology* 79: 15.
- Leite LWB, Leao JWD (1985). Ridge regression applied to the inversion of two-dimensional aeromagnetic anomalies. *Geophysics* 50: 1294-1306.
- Lowrie W (2007). *Fundamentals of Geophysics*. Cambridge, UK: Cambridge University Press.
- Mendonça CA, Silva JBC (1994). The equivalent data concept applied to the interpolation of potential field data. *Geophysics* 59: 722-732.
- Mendonça CA, Silva JBC (1995). Interpolation of potential-field data by equivalent layer and minimum curvature: a comparative analysis. *Geophysics* 60: 399-407.
- Miller HG, Singh V (1994). Potential field tilt—a new concept for location of potential field sources. *Journal of Applied Geophysics* 32: 213-217.
- Nabighian MN, Ander ME, Grauch VJS, Hansen RO, LaFehr TR et al. (2005). Historical development of the gravity method in exploration. *Geophysics* 70: 63ND-89ND.
- Özdemir Y, Karaoğlu Ö, Tolluoğlu AÜ, Güleç N (2006). Volcanostratigraphy and petrogenesis of the Nemrut stratovolcano (East Anatolian High Plateau): the most recent postcollisional volcanism in Turkey. *Chemical Geology* 226: 189-211.
- Parker RL, Klitgord KD (1972). Magnetic upward continuation from an uneven track. *Geophysics* 37: 662-668.
- Paterson N, Reford S, Kwan K (1990). Continuation of magnetic data between arbitrary surfaces: advances and applications. In: *60th Annual International Meeting SEG; San Francisco, USA*. pp. 666-669.
- Pilkington M, Roest W (1992). Draping aeromagnetic data in areas of rugged topography. *Journal of Applied Geophysics* 29 (2): 135-142.
- Pilkington M, Thurston JB (2001). Draping corrections for aeromagnetic data: line versus grid-based approaches. *Exploration Geophysics* 32: 95-101.
- Pilkington M, Boulanger O (2017). Potential field continuation between arbitrary surfaces – comparing methods. *Geophysics* 82: J9-J25.
- Reeves C (2005). *Aeromagnetic Surveys: Principles, Practice and Interpretation*. Netherlands: Geosoft.
- Ridsdill-Smith T, Dentith M (2000). Drape corrections of aeromagnetic data using wavelengths. *Exploration Geophysics* 31: 39-46.
- Robinson ES, Coruh C (1988). *Basic Exploration Geophysics*. New York, NY, USA: Wiley.
- Seven E, Mironov V, Akin K (2019). A new species of *Eupithecia* Curtis (Lepidoptera: Geometridae, Larentiinae). *Zootaxa* 4668: 443-447.
- Syberg FJR (1972). Potential field continuation between general surfaces. *Geophysical Prospecting* 20: 267-282.
- Szitkar F, Dymant J (2015). Near-seafloor magnetics reveal tectonic rotation and deep structure at the TAG (Trans-Atlantic Geotraverse) hydrothermal site (Mid-Atlantic Ridge, 20_N). *Geology* 43: 87-90.
- Tivey MA, Rona PA, Schouten H (1993). Reduced crustal magnetization beneath the active mound, TAG hydrothermal field, Mid-Atlantic Ridge, at 26_N. *Earth and Planetary Science Letters* 115: 101-115.
- Ulusoy İ (2008). *Etude volcano-structurale du volcan Nemrut (Anatolie de l'Est Turquie) et risques naturels associes*. PhD, University of Clermont-Ferrand II, Clermont-Ferrand, France & Hacettepe University, Ankara, Turkey.

- Ulusoy İ, Labazuy P, Aydar E, Ersoy O, Çubukçu E (2008). Structure of the Nemrut caldera (Eastern Anatolia, Turkey) and associated hydrothermal fluid circulation. *Journal of Volcanology and Geothermal Research* 174: 269-283.
- Ulusoy İ, Çubukçu HE, Aydar E, Labazuy P, Ersoy O et al. (2012). Volcanological evolution and caldera forming eruptions of Mt. Nemrut (Eastern Turkey). *Journal of Volcanology and Geothermal Research* 245-246: 21-39.
- Ulusoy İ, Çubukçu HE, Mouralis D, Aydar E (2019). Nemrut Caldera and Eastern Anatolian volcanoes: fire in the highlands. In: Kuzucuoğlu C, Çiner A, Kazancı N (editors). *Landscapes and Landforms of Turkey*. New York, NY, USA: Springer International Publishing, pp. 589-599.
- Walls CC, Hall JM (1998). Interpretation of aeromagnetic anomalies in terms of hydrothermal alteration in Cretaceous normal polarity superchron extrusives of the Troodos, Cyprus, ophiolite. *Journal of Geophysical Research* 103 (2): 30311-30321.
- Verduzco B, Fairhead JD, Green CM (2004). New insights into magnetic derivatives for structural mapping. *The Leading Edge* 23 (2): 116-119.
- Yılmaz, Y, Güner Y, Şaroğlu F (1998). Geology of the Quaternary volcanic centres of the east Anatolia. *Journal of Volcanology and Geothermal Research* 85: 173-210.
- Zhou W (2018) Aeromagnetic Survey. In: Bobrowsky PT, Marker B (editors) *Encyclopedia of Engineering Geology*. Encyclopedia of Earth Sciences Series. Cham, Switzerland: Springer.